The Cryosphere Discuss., 4, 865–900, 2010
www.the-cryosphere-discuss.net/4/865/2010/
doi:10.5194/tcd-4-865-2010

The Cryosphere Discussions

Understanding snow-transport processes shaping the mountain snow-cover

R. Mott, M. Schirmer, M. Bavay, T. Grünewald, and M. Lehning

WSL Institute of Snow and Avalanche Research Davos, Davos, Switzerland

Received: 15 June 2010 – Accepted: 22 June 2010 – Published: 7 July 2010

Correspondence to: R. Mott (mott@slf.ch)

Published by Copernicus Publications on behalf of the European Geosciences Union.

Abstract

Mountain snow-cover is normally heterogeneously distributed due to wind and precipitation interacting with the snow cover on various scales. The aim of this study was to investigate snow deposition and wind-induced snow transport processes on different scales and to analyze some major drift events caused by North-West storms during two consecutive accumulation periods. In particular, we distinguish between the individual processes that cause specific drifts using a physically based model approach. Very high resolution wind fields (5 m) were therefore computed with the atmospheric model Advanced Regional Prediction System (ARPS) and used as input for a model of snow surface processes (Alpine3D) to calculate saltation, suspension and preferential deposition of precipitation. Several flow features during North-West storms were identified with input from a high-density network of permanent and mobile weather stations and indirect estimations of wind directions from snow surface structures, such as snow dunes and sastrugis. We also used Terrestrial and Airborne Laser Scanning measurements to investigate snow deposition patterns and to validate the model. The model results suggest that the in-slope deposition patterns we found, particularly two huge cross-slope cornice-like drifts, developed only when the prevailing wind direction was northwesterly and were formed mainly due to snow redistribution processes (saltation-driven). In contrast, more homogeneous deposition patterns on a ridge scale were formed during the same periods mainly due to preferential deposition of precipitation. The numerical analysis showed that snow-transport processes were sensitive to the changing topography due to the smoothing effect of the snow cover.

1 Introduction

Snow transport processes shape mountain snow-cover during the winter season. The driving force for these processes is the atmospheric boundary layer flow. The mean air flow is modified by the local topography, especially in highly complex terrain. Local

TCD
4, 865–900, 2010

high wind velocities initiate the relocation of snow particles already deposited on the ground, through saltation and suspension processes. Additionally, the interaction of wind and topography during snow-fall promotes enhanced snow loading on leeward slopes due to the preferential deposition of the precipitation (Lehning et al., 2008). These process interactions result in very heterogeneous snow depths and snow cover properties. The heterogeneity of snow-cover properties arising from particular storm events is a special challenge for avalanche forecasting (e.g., Schweizer et al., 2003). The snow distribution at the time of peak accumulation, on the other hand, has a major influence on the timing and the magnitude of snowmelt runoff (Pomeroy et al., 1997; Luce et al., 1998; Liston et al., 2007; Grünewald et al., 2010).

There have been several attempts to provide physically based descriptions of saltation and suspension, which are the main mechanisms for snow transport by wind (Mellor, 1965; Male, 1998; Schmidt, 1986; Pomeroy and Gray, 1990; Lehning and Fierz, 2008). In recent years, more complex model approaches have been developed which use high-resolution atmospheric three-dimensional wind fields to drive the snow-drift models (Gauer, 2001; Liston and Elder, 2006; Lehning et al., 2008). Lehning et al. (2008) introduced the process of preferential deposition of precipitation as an additional mechanism, that influences the distribution when snow is transported by wind.

Wind flow patterns and their related snow-drift processes are highly complex. Moreover, computational costs are high. This is why most attempts to model snow transport by wind have relied on oversimplification, either using simple terrain-based parameters on snow distribution (Purves et al., 1998; Winstral and Marks, 2002; Winstral et al., 2002) or empirical and analytical relationships between topographical parameters, wind velocity and transport rates of snow (Tabler, 1975; Uematsu et al., 1991; Liston et al., 2007). It has been suggested, however, that the driving wind field is the most sensitive parameter for simulating the small-scale distribution of snow (Lehning et al., 2000; Essery, 2001; Raderschall et al., 2008; Dadic et al., 2010a). Thus, an adequate representation of the characteristic flow features for alpine terrain, such as crest separation and flow blocking, is essential for snow-drift modelling on very small scales (tens

TCD
4, 865–900, 2010

of meters). Previously, atmospheric mean flow fields have been successfully used to model snow drifts in very complex terrain (Lehning et al., 2008; Bernhardt et al., 2010; Mott and Lehning, 2010). When atmospheric models were applied to glaciated terrain, it was found that a horizontal grid resolution of 25 m is sufficient to represent ridge-scale deposition features (Mott et al., 2008; Dadic et al., 2010a). There seems to be a strong correlation between the main seasonal accumulation areas on alpine glaciers and increased horizontal and decreased downward surface-normal wind velocities. However, a recent investigation on snow-transport processes suggests that the spatial resolution used in the related numerical analysis is still insufficient to capture the snow-deposition features caused by pure drift processes (Mott and Lehning, 2010). A more realistic representation of the small-scale deposition patterns, such as dunes and cornices, is very sensitive to grid resolution and can only be achieved if a horizontal resolution of 10 m or less is used.

To our knowledge, all previous studies on snow-drift modelling have used horizontal grid resolutions of 25 m or coarser. Furthermore, most of the studies performed in Alpine catchments to date have not used sufficiently dense spatial and temporal measurements of snow depths and meteorological data (e.g., Bernhardt et al., 2010), which makes their promising results difficult to validate. Combining high-resolution measurements of the snow cover with a high density of meteorological stations provides a way to examine the spatial and temporal development of the snow cover (Schirmer et al., 2010b), as well as the driving atmospheric forces for drifting and blowing snow on a very small scale of just a few meters. These measurements also ensure the validation of atmospheric and snow-transport models is adequate and help in analysis of different snow-transport processes.

All measurements were performed in the *Wannengrat* area, located in Davos, Switzerland, which has been successfully established as an investigation area for snow-cover and snow-hydrology related studies (Grünewald et al., 2010; Bellaire and Schweizer, 2010; Schirmer et al., 2010b). In this area we obtained high resolution measurements of snow depths for large snow-fall events during the snow-accumulation

TCD
4, 865–900, 2010

periods of 2008/2009 and 2009/2010. Additionally we measured atmospheric forcing with a very dense measurement network. We also investigated the influence of the changing topography during the accumulation period on the development of drifts observed in the investigation area. Finally, we identified the spatial characteristics of deposition patterns using simple statistics and related them to the main snow-transport mechanisms and their dominance in specific areas which depends on the local wind field.

2 Methods

2.1 Site description, measurements and analysis strategy

Our study site, the *Wannengrat* is near the town of Davos, Switzerland. The whole area is located above the local tree-line at altitudes ranging from 2000 m to 2700 m a.s.l. (Fig. 1). The investigation area is equipped with seven permanent weather stations (WAN 1–7) and an additional 17 mobile stations (SensorScope, Swiss Experiment: www.swiss-experiment.ch), indicated by yellow and red stars in Fig. 1. The SensorScope stations were concentrated around the *Wannengrat ridge*, the *Latschüelfurgga* and on a leeward slope, which we refer to as the *bowl*. All meteorological stations were equipped with wind sensors.

To gain additional information about the local flow direction, we used snow-surface structures, such as snow dunes and sastrugis, as proxy data for wind direction. We expected these structures to allow the locally dominant flow directions to be adequately identified and thus provide further verification for numerical wind field simulations for specific areas. The appearance of surface structures, could also be used to distinguish areas of low and high wind velocities. These proxy data from the snow surface were based on orthophotos with a pixel resolution between 7 and 9 cm, obtained from the TLS surveys. We chose orthophotos obtained from the first measurement campaign for one typical event in October 2009 since sastrugis were well developed after the

TCD
4, 865–900, 2010

snow-fall event. Wind data during North-West (NW) storms tend to be very consistent (see Sect. 3.1.), which meant we could assume that these surface structures would be representative for all NW storms.

Snow depths were measured with a terrestrial laser scanner (Riegl LPM-321) before and after several drift events in winter 2008/2009 and winter 2009/2010 (Fig. 2). Additionally the snow depth distribution was measured at the time of peak accumulation (HS_{max} situation) for the winters 2007/08, 2008/09 and 2009/10. A detailed description of the measurement set-up and error estimation of the TLS in the *Wannengrat* area can be found in (Grünewald et al., 2010). For more general discussions of the application of laser-scanning technology to snow depth measurements, see (Prokop et al., 2008) and (Schaffhauser et al., 2008). The final raster maps of snow depth (HS) and snow depth change (dHS) due to individual snow-drift events had a cell size of 1 m for each survey. To cover a larger area without measurement gaps, the snow depths (HS_{max}) were also measured using airborne laser scanning (ALS) at the time of the peak accumulations in 2007/2008 and 2008/2009. For these two campaigns a helicopter based technology (Skaloud et al., 2006) was used. (Grünewald et al., 2010) studied both methods and found a mean error of HS in the order of centimeters. The first series of TLS measurements in the *Wannengrat* area revealed a very strong inter-annual consistency between the HS_{max} situations of the winter 2007/2008 and 2008/2009 (Schirmer et al., 2010b). The correlations between the two HS_{max} situations were r=0.97 on the *NE slope* and r=0.93 in the *bowl*. The NW storms correlated strongly with these HS_{max} situations, with r=0.88 for the first NW storm ($P1_{0809}$) of the winter 2008/09 and r=0.76 for the last NW storm of this winter ($P8_{0809}$). The snow deposition patterns found after NW storms were very similar and they contributed significantly to the final snow depth distribution at the HS_{max} situation. We therefore only focused on those drift events caused by NW storms (Fig. 2). To examine these typical events, we selected three drift events in 2008/2009 and three drift events in 2009/2010 affected by NW storms.

TCD
4, 865–900, 2010

2.2 Model set-up for flow field and drift simulations

We calculated the mean flow fields with the non-hydrostatic and compressible atmospheric model ARPS, developed at the Center for Analysis and Prediction of Storms (CAPS), University of Oklahoma (Xue et al., 2004). We were only interested in the mean wind fields because measurements showed very consistent mean hourly wind directions during NW storms. Therefore we assume that these mean wind fields may explain observed deposition patterns consistent with our earlier results (Raderschall et al., 2008; Mott and Lehning, 2010; Dadic et al., 2010a).

The ARPS model was initialized using horizontally homogeneous fields and artificial vertical profiles of the atmosphere, which described the atmosphere for a characteristic situation during snow fall. The atmosphere was assumed to be slightly stably stratified and nearly saturated. We used a standard logarithmic profile of the horizontal wind within the boundary layer and defined a vertically constant free-stream velocity above the boundary layer. The height of the boundary layer was set to 500 m. For all model runs, a snow-covered topography was taken into consideration by using an aerodynamic roughness length of z_0=0.01 m (Doorshot et al., 2004; Stössel et al., 2010). We used a zero-gradient formulation for the upper boundary. The bottom boundary conditions were defined as a rigid wall, and for the lateral boundaries periodic boundary conditions were used.

To compute mean flow features, we ran the model for rather short integration times of 30 s, which ensured that the flow was not dominated by turbulent structures and the model remained stable in the face of periodic boundary conditions. The influence of the integration time and boundary conditions on flow adaptation is discussed in detail in Raderschall et al. (2008). The domain covered the surrounding topography of the *Wannengrat* area, which is considered to have a major influence on the flow field within the investigation area. The domain size was accordingly set to 2.5×2.8 km. To test the influence of the changing topography, we also performed wind simulations for the winter topography of 2009. Two digital elevation models, the DEM_S and the

TCD
4, 865–900, 2010

DEM_W, were created by a resample of a high resolution airborne laser scan to a 5 m grid. The DEM_S was taken in summer 2009, while the DEM_W was taken at the time of peak accumulation on 9 April 2009. The DEM_S therefore represents the summer topography and the DEM_W the winter topography. The ARPS model uses a terrain following coordinate system. The finest vertical grid resolution of about 0.8 m is found close to the ground.

In total five wind fields were modelled, initiated with wind velocities varying between very low (2 m/s) and very high (9 m/s) at 2400 m a.s.l. The model output is a three-dimensional grid of velocity with x,y,z vectors, which was then used as input for the snow-transport model of Alpine3D (Lehning et al., 2008). In this model, the redistribution of snow is calculated as composed of the pure drift processes, saltation and suspension, and preferential deposition of precipitation (Clifton and Lehning, 2008; Lehning et al., 2008). To distinguish between the different wind-induced snow-transport processes, the model allows the process of preferential deposition of precipitation to be calculated separately from saltation and suspension.

Since this study aims to deal with all processes that cause the spatial and temporal variability of the snow depth, we used a full description of the energy balance at the snow surface as implemented in Alpine3D (Helbig et al., 2008). The energy balance model and snow-transport model are fully coupled to the snow-cover module SNOWPACK (Lehning and Fierz, 2008). This particular model set-up enabled us to account for the influence of the local energy balance on the snow-cover properties and therefore also on the snow-drift processes. One hour was chosen as a suitable model time step. Apart from the three-dimensional wind fields, we initialized Alpine3D with hourly meteorological data, gained from two permanent meteorological stations (WAN3, WAN7) within the investigation area (Fig. 1). We assumed relative humidity to be homogeneously distributed over the domain, while air temperature and long-wave radiation were distributed over the computational domain with an altitudinal gradient. The actual state of the homogeneously distributed snow-cover properties at the start of snow-fall event was initialized by vertical profiles of the snow cover, calculated with

TCD
4, 865–900, 2010

the one-dimensional SNOWPACK module for a flat field station (WAN 7, Fig. 1) within the study area. The three-dimensional wind fields obtained from ARPS were chosen using a classification schema based on the frequency distribution of wind velocity at the reference wind station (WAN 2, Fig. 1) for the specific periods.

We used two different topographies, the DEM_S and DEM_W, for atmospheric simulations. In general, the simulations of the first drift events of the two accumulation periods were driven by flow fields calculated over summer terrain (DEM_S), while the drift periods at the end of the accumulation season were simulated using flow fields calculated over winter terrain (DEM_W).

The spatial variability of the modelled and observed snow depth changes (dHS) is explored using simple statistics, such as the mean (μ) and standard deviation (σ). To calculate the relative contribution of the redistribution processes (saltation and suspension) versus the preferential deposition of precipitation, we had to perform two different simulation runs for each period. We ran the model either with all wind-induced snow-transport processes (dHS_{all}) or only with the preferential deposition of precipitation (dHS_{prec}).

3 Results and discussion

3.1 Flow field: observed and modelled

In Fig. 3 wind roses for three permanent stations for the three NW storms in winter 2008/2009 are illustrated. We averaged the wind data to 10 min intervals. The plot impressively demonstrates the clear prevailing wind directions for each station for all three NW storms. This time consistency of the prevailing wind directions during NW is also shown by nearly all stations located in the *Wannengrat* area, except those which are situated in flow separation zones. It is worth noting that the wind directions are stable over time, but vary strongly between the stations, from North-West at station WAN 1 to South-West at station WAN 6, as indicated by the terrain.

TCD
4, 865–900, 2010

A map of the most frequently measured wind directions at each station for a snow-fall event (without precipitation) in January 2010 is shown in Fig. 4a. This snow-fall event $P3_{0910}$ occurred during a synoptically controlled NW wind situation. The length and the color of the wind vectors represent mean wind velocities for the period of 24 h during 28 January 2009. The wind directions obtained from snow-surface structures as described above are indicated with black arrows. The measurements revealed very characteristic flow patterns with a clear influence of the local topography. Despite the time stability of wind directions for the single stations, the local wind patterns varied considerably over small distances of a few hundred meters. On ridges we consistently observed a flow perpendicular to the ridge. This also includes the flow turning to a southwesterly flow at WAN 5 and WAN 6 and on the slope north of *Latschüelfurgga* (Fig. 4a). In contrast, the mobile stations and proxy data of the *NW slope* displayed evidence of a flow around the *Wannengrat* ridge with a southwesterly flow in the lower parts of the *NW slope*. The main flow on *Chilcher Berg* and *Latschüelfurgga* was northwesterly due to channelling (WAN2, WAN3). The mobile stations and proxy data on the *NE slope* showed a clear northwesterly wind direction. Within the *bowl*, in contrast, we did not observe such stable wind patterns. Within a small time span of one hour, the flow directions in the wind-sheltered area vary between southeasterly and southwesterly flows with rather low wind speeds. These varying wind directions and low wind speeds are a clear sign of flow separation on the ridge of *Chüpfenflue*.

The highest wind velocities were observed on the ridges and on the *Latschüelfurgga* due to speed-up effects and flow channeling. Increased wind velocities were observed at wind-exposed stations located on bumps and lower wind velocities at those situated in wind-sheltered terrain depressions. Well-developed surface structures due to wind were formed on the *NE slope*, *NW slope* and the *SW slopes*, which indicates increased wind velocities in these areas. On the *NE slope* the surface structures developed more strongly on the windward than on the leeward sides of the two ridges, which indicate high and low wind velocities, respectively. In contrast, no surface structures were formed within the *bowl*, which clearly suggested low wind velocities in this area.

TCD
4, 865–900, 2010

In Fig. 4b, the modelled mean flow field for a characteristic NW storm with moderate wind velocities is illustrated. A qualitative comparison between the observed mean flow direction and the simulated mean flow direction tended to agree well for all ridges, with observed flow perpendicular to the ridge. In general, the flow turn to southwest is well presented in the model results, even if the turn to southwest is not as strong as actually shown by the measurements. Furthermore, the simulations are able to capture the flow around the *Wannengrat*. The numerical analysis indicated that this flow is caused by the flow blocking on the lower parts of the *NW slope*, it presumably developed when there was a slightly stable atmospheric stratification of the atmosphere, mostly found during snow-drift events. The flow around the Wannengrat is marked by strong speed-up, which may also enhance the flow on the *NE slope*. A quantitative evaluation of the modelled wind directions showed that, at these locations, where the flow was within the West-Northwest sector, the mean deviation between the modelled and the measured mean wind direction was only 6 degrees for all stations. In contrast, the mean deviation at locations where the flow turned to southwest was 17 degrees. Stations located within the *bowl* were removed from statistical analysis as they are strongly influenced by turbulence.

In general, the wind velocity distribution is well captured by the model, even if the speed-up effects on the ridges are too high at some locations. The simulation results show increased wind speeds for the ridges and bumps, and decreased wind speeds on leeward slopes. The wind-sheltered *bowl*, the *Vorder Latschüel* and the *Steintäli*, are characterized by very high wind velocities on the ridges and very low wind velocities within the two *bowls*.

3.2 Snow deposition patterns caused by the local flow field

3.2.1 Snow deposition patterns (observed and modelled)

Change in snow depth (dHS) caused by NW storms are shown in Fig. 5. We can distinguish between different sub-areas according to the snow-depth distribution (Fig. 5).

TCD
4, 865–900, 2010

The typical snow depth distribution is discussed in detail by Schirmer et al. (2010b) and Schirmer and Lehning (2010). The *bowl* is characterized by homogeneous lee-slope loading, with somewhat enhanced snow deposition in narrow channels. The *NW slope* is dominated by wind erosion (Fig. 5b), with one main deposition zone located on a terrain depression. In contrast, the *NE slope* is a cross-loaded slope, with a very high spatial variability of dHS. On this slope, two huge accumulation zones developed every winter in the lee of two cross-slope ridges of summer terrain. These accumulation zones were formed during NW storms, when the flow is perpendicular to these ridges, and were interpreted as cornice-like drifts (Fig. 5b). The flatter terrain (*SW slopes*) is strongly characterized by snow filled channels, dells and eroded bumps (Fig. 5b).

A qualitative comparison of the measured snow deposition patterns and the simulated dHS after NW storms (Fig. 6) showed that the model is able to capture typical snow deposition patterns (Fig. 5). These are the large accumulation zones (cornice-like drifts) in the lee of the cross-slope ridges on the *NE slope*, the erosion zones on the *NW slope* and most of the deposition zones on the *SW slopes*. The reduced snow deposition on the top of the *NE slope* is not captured nor is the filling of channels on the flatter terrain (*SW slopes*). Since measurements for the *NW slope* are not available for all events, we will not discuss this sub-area in more detail in the later sections.

The measurements and model results (Fig. 5) showed that the NW storm periods of 2008/2009 formed more significant deposition patterns than those of 2009/2010. The cornice-like drifts were modelled mainly during snow-fall events with wind velocities high enough to initiate snow drift ($P1_{0809}$, $P7_{0809}$, $P8_{0809}$, $P1_{0910}$). In periods with lower wind velocities, for example, $P4_{0910}$ (Fig. 6f), snow-transport processes could not be initiated to form the cornice-like drifts. Note that the erosion zones, which are visible in the map of measured dHS of $P4_{0910}$ (Fig. 5f, red colors), are due to avalanches which occurred during this short period. The magnitude of snow deposition and therefore the continuous formation of the cornice-like drifts strongly depend on the forcing wind velocity. The snow redistribution is a non-linear function of wind velocity (Doorschot et al., 2004). In Fig. 7, dHS at the cornice-like drifts is plotted for snow drift events with

TCD
4, 865–900, 2010

high (initialized wind velocity was 7 m/s) and moderate (initialized wind velocity was 4 m/s) wind velocities. A very large increase in absolute snow deposition, as well as an increase of variance in dHS with wind velocity is clearly visible.

3.2.2 Influence of the surface modification on snow-transport processes

The change in snow depth for the whole model domain are shown in Fig. 8a for $P7_{0809}$ simulated over summer terrain (DEM_S). Due to the significant contribution of NW storms to the final snow depth distribution for the HS_{max} situation, we compare modelled dHS to measured HS at the HS_{max} situation 2008/2009 (Fig. 8c), obtained from the airborne laser scan. Many of the observed and modelled deposition patterns are similar, see Fig. 8 where some of these patterns are shown with colored circles. It should be noted that a huge avalanche occurred in the *bowl* in March 2009, which resulted in different snow deposition patterns in the outrun zone, as well as less snow within the *bowl*. The avalanche cannot be captured by the model.

Various modelled deposition patterns were obtained when the same period $P7_{0809}$ was simulated over winter terrain (DEM_W) (Fig. 8b). The variability of dHS is lower for simulation runs performed over winter topography. This is consistent with the observations of Schirmer et al. (2010b), who showed that the variance of dHS due to NW storms tends to decrease during the winter. The modification of the terrain surface due to the snow cover may have a major effect on the local wind field, and thus on the snow distribution after the NW storms. The results from flow-field simulations using the different topographies (not shown) demonstrate a significant influence of the effect of the snow-covered terrain on the flow field. The wind velocity distribution simulated with the DEM_W (not shown) also became less variable because of the filling of the terrain depressions. On the other hand, wind velocities became more pronounced in enhanced snow deposition zones, for example on developed cornices. Consequently, the modelled snow depth changes also tend to become smoothen towards the end of the accumulation season, especially in the flatter areas, which are dominated by smaller-scale surface structures (Fig. 8b). However, the dominant deposition zones

TCD
4, 865–900, 2010

(e.g. cornice-like drifts), as well as the ridge-scale deposition features within the *bowl*, were still modelled.

We examined the temporal development of the cross-slope cornices and its dependence on the surface modification in more detail. In Fig. 9 the temporal evolution of the snow cover on the cornice-like drifts for the accumulation period 2008/09 is shown along a transect line (indicated in Fig. 1). What is clearly visible is that the two cornice-like drifts grew consistently in the course of the accumulation period and the crowns moved in the flow direction. However, the first cornice-like drift grew less than the second. We attribute the different growth dynamics of the two drifts to the fact that snow-deposition processes continuously modified the topography. After the first snow fall of the year, the surface was very rough and then smoothed in the course of the accumulation season. The strong gradient of the slope on the leeward side of the first ridge was strongly smoothed and flattened by snow deposition (Fig. 10a), while the leeward slope of the second drift even slightly increased. The reaction of the flow field and resulting modelled changes in snow depth to the surface modification is analyzed in Fig. 10. The wind field over summer terrain showed increased wind velocities on both ridges and decreased wind velocities in the leeward slopes of these ridges, which resulted in strong gradients of wind velocity. Over winter terrain, the speed-up effects of the wind became less pronounced (Fig. 10b) on the first ridge. The wind simulation on the second ridge also changed to less speed-up, but a high gradient in wind speed was maintained. The snow-drift processes were active on the second ridge, whereas the snow-redistribution processes acting on the first drift became weaker with time (Fig. 10c). For both drifts, the peak of deposition (i.e. the crown) was shifted about 30 m in the flow direction. In summary, the snow-drift simulations showed that the snow depth distribution is very sensitive to modifications of the wind due to the local topography, while the topography is consistently modified by snow-transport processes itself. This indicated that the mechanisms of snow-transport processes shaping the mountain snow-cover are strongly self-regulating.

TCD
4, 865–900, 2010

3.2.3 Wind-induced snow-transport processes driving the snow deposition in different sub-areas

In this subsection we want to discuss the dominance of the different processes that drive snow transport, namely saltation, suspension and preferential deposition of precipitation, in different sub-areas within the Wannengrat area. To test whether these processes affect the spatial variability of snow depths in the sub-areas: the *bowl*, the *NE slope* and the *SW slopes* (Fig. 1), we applied simple statistics, standard deviation (μ) and mean (σ), to the measured dHS, modelled dHS_{prec} and dHS_{all}.

In Fig. 11, μ of dHS is given for the whole area for the three drift events in 2008/09 and the model results are compared with the measurements. The simulation results showed a similar trend with a decreasing variance of dHS_{all} and dHS_{prec} during the winter, associated with the effect of the changing topography on the local wind field (see Sect. 3.2.2). The mean and the standard deviation of dHS for the sub-areas are given in Fig. 12. Measurements showed that the snow cover of the *bowl* was characterized by the highest μ, but the lowest σ (Fig. 12a,b). In contrast, for the *NE slope* μ was low, but the spatial variability (σ) of the snow cover was the highest. The modelled dHS_{all} results in overestimates of μ (Fig. 12c) and σ (Fig. 12d) for the *bowl*. These are consistent with the overestimation of the wind sped, as discussed above, and could be explained by the development of unrealistically large cornices on the ridge of the Chüpfenflue which primarily arise from saltation processes. We therefore introduced a fourth sub-area, the *inner bowl*. If we analyze the *inner bowl* separately, the variance of dHS_{all} becomes very low. The highest σ (Fig. 12d) and the lowest μ (Fig. 12c) were calculated for the *NE slope*.

The simulations of the preferential deposition of precipitation suggested a strong decrease in the total variance (Fig. 12f). For the sub-areas, the modelled dHS_{prec} captured the spatial variability very well for the *bowl* (Fig. 12b, g), but not for the *NE slope*. Therefore the preferential deposition of precipitation appeared to be the dominant snow-transport mechanism, causing the low spatial variability of dHS within the

TCD
4, 865–900, 2010

bowl after NW storms (Fig. 12b). In contrast, the high variability of dHS on the *NE slope* after NW storms (Fig. 12b) could mainly be explained by pure snow drift, i.e. snow redistribution, (Fig. 12c, d), which led to the formation of the cornice-like drifts.

The relative importance of these transport processes in different areas is related to the local wind field as a function of the local topography. In Fig. 13, the modelled dHS_{prec} for $P1_{0809}$ (a) and the spatial distribution of the three-dimensional wind velocity (b) and the vertical component of wind velocity (c) are shown for one wind field (initialized wind velocity was 5 m/s). The flow field simulations (Figs. 4b, 13b) showed that, during synoptically controlled NW flow, the *bowl* was characterized by a high wind velocity gradient on the leeside of the ridge. In the *inner bowl*, modelled wind velocities were very low with a very homogeneous distribution of wind velocity (Fig. 13b) and vertical wind velocity (Fig. 13c). The negative vertical wind velocities indicate a downdraft zone within the whole *bowl*. The modelled decreased wind velocities and downdrafts indicate that preferential deposition of precipitation is the dominant snow deposition mechanism in the *bowl* (Figs. 12e, 13a). This leads to a more homogeneous lee-slope loading (Lehning et al., 2008) and corresponds with the low variance in snow depth changes observed in the *bowl* (Fig. 12b,f). For the *NW slope*, the numerical analysis suggests that the flow around the Wannengrat and the associated local speed-up caused an enhanced flow on the *NE slope*. This led to high wind speeds on the windward sides and decreased wind speeds on the leeward sides of the cross-slope ridges. This flow field resulted in pronounced erosion on the windward sides and enhanced deposition on the leeward sides of the cross-slope ridges. Thus a high spatial variability of the wind field (Fig. 13b) caused considerable redistribution of snow, resulting in a high variance of dHS on the *NE slope* (Fig. 12b,d) and the formation of huge drifts. The simulation results suggests that these cornice-like drifts, especially the formation of the crowns, were simulated mainly due to snow redistribution processes (e.g., Fig. 12d).

The strong relationship between the local flow field and the snow depth changes could be confirmed in a correlation analysis for the transects crossing the *NE slopes* (Fig. 1). In Table 1 the correlation coefficients between the modelled wind field and

TCD
4, 865–900, 2010

the measured dHS, as well as for the modelled dHS_{all} and the measured dHS are given. All the correlation values were calculated for the three transects crossing the cornice-like drifts in the flow direction (Fig. 1) and for the drift periods $P1_{0809}$ and $P8_{0809}$. High positive correlations between the modelled and the measured dHS suggest that the cornice-like drifts were well-captured by the model, especially at the end of the accumulation period. The correlation coefficients for $P1_{0809}$ were lower because the cornice-like drift on the first ridge was simulated too close to the ridge. Furthermore there were high negative correlation coefficients between the three-dimensional wind velocity and the measured dHS for $P1_{0809}$ and $P8_{0809}$. This is in accord with the strong correlation between low wind velocities behind the ridges and increased deposition of snow in these areas, while the increased wind velocity due to speed-up effects resulted in more erosion on the windward sides of the cross-slope ridges. Even higher negative correlation coefficients were found for the vertical wind velocity, which reflects the strong correlation between downdraft zones (negative vertical wind velocity) and increased deposition of snow. These correlations confirm earlier results on a larger scale (Dadic et al., 2010a) and encourage the development and use of simple parameterization schemes (Dadic et al., 2010b).

4 Conclusions

These results from flow and snow-transport modelling, help to explain individual snow-transport processes during NW storms. This study drew on the findings of Schirmer et al. (2010b), who showed that the final snow distribution at the time of peak accumulation is mainly shaped by “master” storms (i.e. NW storms) and that these storms created persistent accumulation patterns. We have been able to demonstrate that most snow deposition patterns found at the time of peak accumulation can be explained and modelled with the help of a few mean flow fields calculated by ARPS. Our numerical analysis shows that these storms produce very characteristic flow patterns, with small-scale flow features such as local speed-up effects developing over sub-slope terrain

TCD
4, 865–900, 2010

structures (e.g. cross-slope ridges) and ridge-scale flow features, such as flow blocking or wind separation developing as a result of larger-scale terrain features. These flow features on different scales appear to be very important for different snow-transport processes. The drift simulations suggest that the snow distribution of the *NE slope* is governed mainly by saltation/suspension processes, while that in the *bowl* is mainly influenced by preferential deposition of precipitation. In particular, two huge cross-slope cornice-like drifts on the *NE slope* developed only when the prevailing wind direction was NW and were formed mainly through snow redistribution processes (saltation-driven).

Changing topography was also found to have a significant effect on the flow field and the final snow distribution. The modification of the topography has been found to be the main reason for the decrease in variance of observed snow depths caused by NW storms during the winter. Over winter terrain, smaller-scale terrain features were not present anymore and therefore only the larger-scale terrain features continued to shape flow field modification and the associated snow deposition. In contrast, very small-scale and larger-scale terrain features had a considerable impact on the flow field over summer terrain resulting in a very variable snow depth distribution and saltation becoming more important. The dynamics of the drift formation strongly depend on the feedback between snow deposition processes, the changing topography and the local wind field, especially for the temporal development of the cornice-like drifts.

Schirmer et al. (2010b) tried to reproduce the spatial patterns of snow-depth distribution using a simple terrain analysis (Winstral et al., 2002), and were in fact able to produce the main spatial patterns. They failed, however, to reproduce the magnitude of the observed variability. In contrast, the physical approach we used captured the effect of a non-linear response of snow-transport processes to wind velocity variations and allowed the individual processes involved to be separated. The main advantage of our study is that our description of snow depth variability is process-oriented. We are able to show that special flow conditions always lead to similar deposition patterns, which should provide a basis for simpler parameterizations of snow deposition caused by drift

TCD
4, 865–900, 2010

and the preferential deposition of precipitation such as already attempted by Dadic et al. (2010b).

The main purpose of this investigation was to use physical modelling to explain observed variability of snow depths as shaped by individual storms during the accumulation period. As a next step, we plan to investigate how the local flow field affects the scaling characteristics of the snow depths caused by NW storms. In particular, we are interested if we can find coherent scaling parameters between the spatial distribution of snow depths and wind speeds. We note that we only work with mean flow fields and do not explicitly consider the highly turbulent flow nor the mostly intermittent snow transport. A logical further step would therefore be to make use of the advanced performance of LES simulations (Chamecki et al., 2008) to investigate the limits of our equilibrium descriptions. We further note that we have not simulated a full time development of the snow cover and in particular for the purpose of slope stability estimations based on weak layer modelling (Schirmer et al., 2010a), this would be a mandatory requirement, which we want to tackle in our continuing effort.

Acknowledgements. The wind simulations were made using the Advanced Regional Prediction System (ARPS) developed by the Center for Analysis and Prediction of Storms (CAPS), University of Oklahoma. Part of the work was funded by the Swiss National Science Foundation and the European Community (FP7 project HYDROSYS). We are grateful to our colleagues who helped during the field campaigns, especially Vanessa Wirz and Luca Egli.

References

Bellaire, S. and Schweizer, J.: Estimating slope stability from spatial snow cover observations, submitted to Cold Reg. Sci. Technol., 2010. 868

Bernhardt, M., Liston, G. E., Strasser, U., Zángl, G., and Schulz, K.: High resolution modelling of snow transport in complex terrain using downscaled MM5 wind fields, The Cryosphere, 4, 99–113, doi:10.5194/tc-4-99-2010, 2010. 868

Chamecki, M., Meneveau C., and Parlange, M. B.: A hybrid spectral/finite-volume algorithm for large eddy simulation of scalars in the atmospheric boundary layer, Bound.-Lay. Meteorol., 128(3), 473–484, 2008. 883
Clifton, A. and Lehning, M.: Improvement and validation of a snow saltation model using wind tunnel measurements, Earth Surf. Proc. Land., 33, 2156–2173, 2008. 872
Dadic, R., Mott, R., Lehning, M., and Burlando, P.: Wind influence on snow depth distribution and accumulation over glaciers, J. Geophys. Res., 115, F01012, doi:10.1029/2009JF001261, 2010. 867, 868, 871, 881
Dadic, R., Mott, R., Lehning, M., and Burlando, P.: Parameterization for wind-induced preferential deposition of snow, Hydrol. Process., in press, 2010. 881, 883
Doorschot, J., Lehning, M., and Vrouwe, A.: Field measurements of snow drift threshold and mass fluxes, and related model simulations, Bound.-Lay. Meteorol., 113(3), 347–368, 2004. 871
Essery, R.: Spatial statistics of wind flow and blowing snow fluxes over complex terrain, Bound.-Lay. Meteorol., 100, 131–147, 2001. 867
Gauer, P.: Numerical modelling of blowing and drifting snow in Alpine terrain, J. Glaciol., 47(156), 97–110, 2001. 867
Grünewald, T., Schirmer, M., Mott, R., and Lehning, M.: Spatial and temporal variability of snow depth and ablation rates in a small mountain catchment, The Cryosphere, 4, 215–225, doi:10.5194/tc-4-215-2010, 2010. 867, 868, 870
Helbig, N., Löwe, H., and Lehning, M: Radiosity approach for the shortwave surface radiation balance in complex terrain, J. Atmos. Sci., 66, 2900–2912, 2009. 872
Lehning, M., Doorschot, J., and Bartelt, P.: A snow drift index based on SNOWPACK model calculations, Cold Reg. Sci. Technol., 31, 382–386, 2000. 867
Lehning, M., Löwe, H., Ryser, M., and Raderschall, N.: Inhomogeneous precipitation distribution and snow transport in steep terrain, Water Resour. Res., 44, W09425, doi:10.1029/2007WR006544, 2008. 867, 868, 872, 880
Lehning, M. and Fierz, C.: Assessment of snow transport in avalanche terrain, Cold Reg. Sci. Technol., 51, 240–252, doi:10.1016/j.coldregions.2007.05.012, 2008. 867, 872
Liston, G. E. and Elder, K.: A meteorological distribution system for high-resolution terrestrial modeling (MicroMet), J. Hydrometeorol., 7(2), 217–234, 2006. 867

TCD
4, 865–900, 2010

Liston, G. E., Haehnel, R. B., Sturm, M., Hiemstra, C. A., Berezovskaya, S., and Tabler, R. D.: Instruments and methods simulating complex snow distributions in windy environments using SnowTran-3D, J. Glaciol., 53(181), 241–256. 2007. 867

Luce, C. H., Tarboton, D. G., and Cooley, K. R.: The influence of the spatial distribution of snow on basin-averaged snowmelt, Hydrol. Process., 12(10–11), 1671–1683, 1998. 867

Male, D. H.: The seasonal snowcover, in: Dynamics of Snow and Ice Masses, edited by: Colbeck, S. G., Academic Press, 305–395, 1980. 867

Mellor, M.: Blowing Snow, CRREL, Monogr. III-A3c, 1965. 867

Mott, R., Faure, F., Lehning, M., Löwe, H., Hynek, B., Michlmayr, G., Prokop, A., and Schner, W.: Simulation of seasonal snow-cover distribution for glacierized sites on Sonnblick, Austria, with the Alpine3D model, Ann. Glaciol., 49, 155–160, 2008. 868

Mott, R. and Lehning, M.: Meteorological modelling of very-high resolution wind fields and snow deposition for mountains, J. Hydrometeorol., in press, doi:10.1175/2010JHM1216.1, 2010. 868, 871

Pomeroy, J. W. and Gray, D. M.: Saltation of snow, Water Resour. Res., 26(7), 1583–1594, 1990. 867

Pomeroy, J. W., Marsh, P., and Gray, D. M.: Application of a distributed blowing snow model to the Arctic, Hydrol. Process., 11(11), 1451–1464, 1997. 867

Prokop, A., Schirmer, M., Rub, M., Lehning, M., and Stocker, M.: A comparison of measurement methods: terrestrial laser scanning, tachymetry and snow probing, for the determination of spatial snow depth distribution on slopes, Ann. Glaciol., 49, 210–216, 2008. 870

Purves, R., Barton, J., Mackaness, W., and Sugden, D.: The development of a rule-based spatial model of wind transport and deposition of snow, Ann. Glaciol., 26, 197–202, 1998. 867

Raderschall, N., Lehning, M., and Schär, M.: Fine-scale modeling of the boundary layer wind field over steep topography, Water Resour. Res., 44, W09425, doi:10.1029/2007WR006544, 2008. 867, 871

Schaffhauser, A., Adams, M., Fromm, R., Jörg, P., Luzi, G., Noferini, L., and Sailer, R.: Remote sensing based retrieval of snow-cover properties, Cold Reg. Sci. Technol., 54(3), 164–175, 2008. 870

Schirmer, M., Lehning, M., and Schweizer, J.: Statistical evaluation of local to regional snowpack stability using simulated snow-cover data, Cold Reg. Sci. Technol., in press, doi:10.1016/j.coldregions.2010.xxxx, 2010a. 883

TCD
4, 865–900, 2010

Schirmer, M., Wirz, V., Clifton, A., and Lehning, M.: Persistence in intra-annual snow depth distribution, Part 1: Measurements and topographic control, submitted to Water Resour. Res., 2010b. 868, 876, 877, 882
Schirmer, M. and Lehning, M.: Persistence in intra-annual snow depth distribution, Part 2: Fractal analysis of snow depth development, submitted to Water Resour. Res., 2010. 876
Schmidt, R. A.: Transport rate of drifting snow and the mean wind speed profile, Bound.-Lay. Meteorol., 34(3), 213–241, 1986. 867
Schweizer, J., Jamieson, B., and Schneebeli, M..: Snow avalanche formation, Rev. Geophys., 41(4), 1016, 2003. 867
Skaloud, J., Vallet, J., Keller, K., Veyssiere, G., and Kölbl, O.: An eye for landscapes – rapid 15 aerial mapping with handheld sensors, GPS World, 17, 26–32, 2006. 870
Stössel, F., Manes, C., Guala, M., Fierz, C., and Lehning, M.: Micrometeorological and morphological observations of surface hoar dynamics on a mountain snow-cover, Water Resour. Res., doi:10.1029/2009WR008198, in press, 2010. 871
Tabler, R. D.: Predicting profiles of snowdrifts in topographic catchments, P. West. Snow Conf., 43, 87–89, 1975. 867
Uematsu, T., Nakata, K., Takeuchi, K., Arisawa, Y., and Kaneda, Y.: Three-dimensional numerical simulation of snowdrift, Cold Reg. Sci. Technol., 20(1), 65–73, 1991. 867
Winstral, A. and Marks, D.: Simulating wind fields and snow redistribution using terrain-based parameters to model snow accumulation and melt over semi-arid mountain catchment, Hydrol. Process., 16(18), 3583–3603, 2002. 867
Winstral, A., Elder K., and Davis, R. E.: Spatial snow modeling of wind-redistributed snow using terrain-based parameters, J. Hydrometeorol., 3(5), 524–538, 2002. 867, 882
Xue, M., Droegemeier, K. K., Wong, V., Shapiro, A., and Brewster, K.: The Advanced Regional Prediction System (ARPS) – A multi-scale non-hydrostatic atmospheric simulation model, Part 2: Model physics and applications, Meteorol. Atmos. Phys., 76, 143–165, 2004. 871

TCD
4, 865–900, 2010

Table 1. Pearsons linear correlation coefficient of measured snow depth change (dHS) against modelled dHS, wind velocity and vertical wind velocity

	$P1_{0809}$			$P8_{0809}$		
Transects	T1	T2	T3	T1	T2	T3
dHS	0.25	0.56	0.27	0.64	0.59	0.75
wind velocity	−0.44	−0.56	−0.65	−0.37	−0.6	−0.51
vertical wind velocity	−0.7	−0.53	−0.62	−0.69	−0.45	−0.7

TCD
4, 865–900, 2010

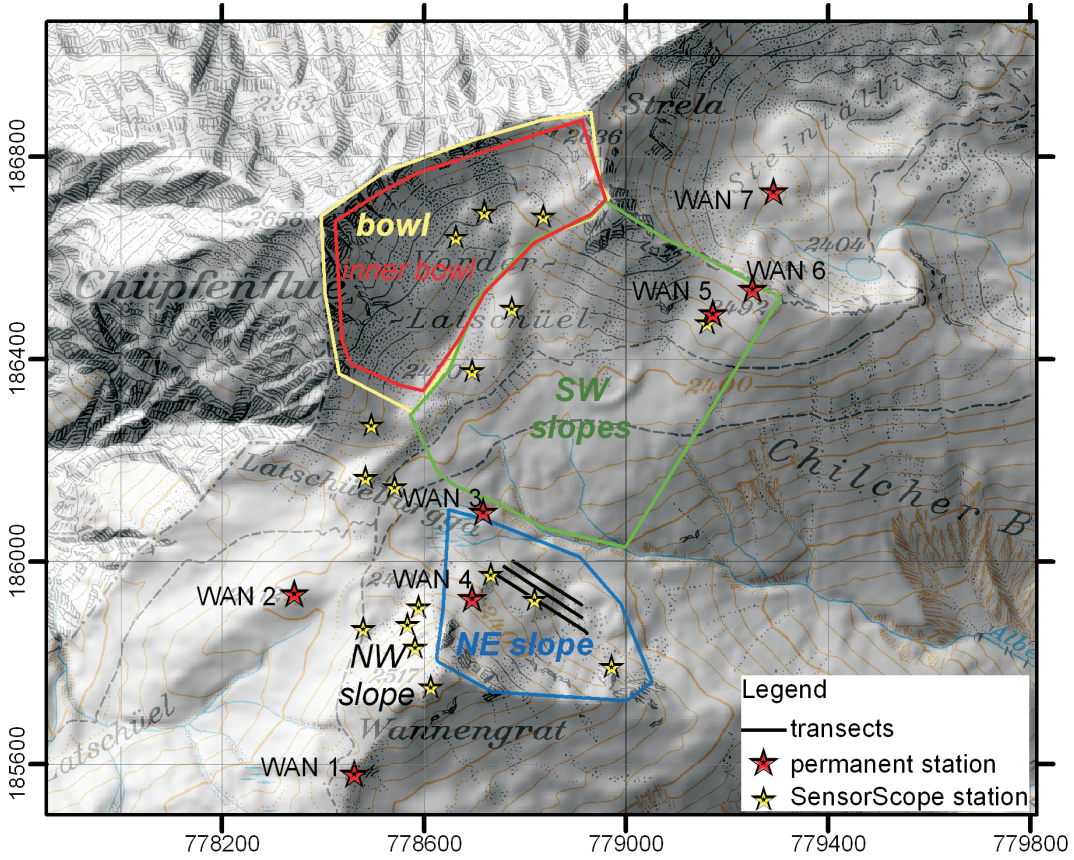

Fig. 1. Location of the study site in the Wannengrat area near Davos. Colored areas indicate the three sub-areas investigated. SensorScope stations are marked with yellow stars and permanent weather stations (WAN 1–7) are marked with red stars. The three black lines mark the transects shown in Figs. 10, 12 and 13, numbered from 1 (the lowest transect) to 3 (the highest transect).

TCD
4, 865–900, 2010

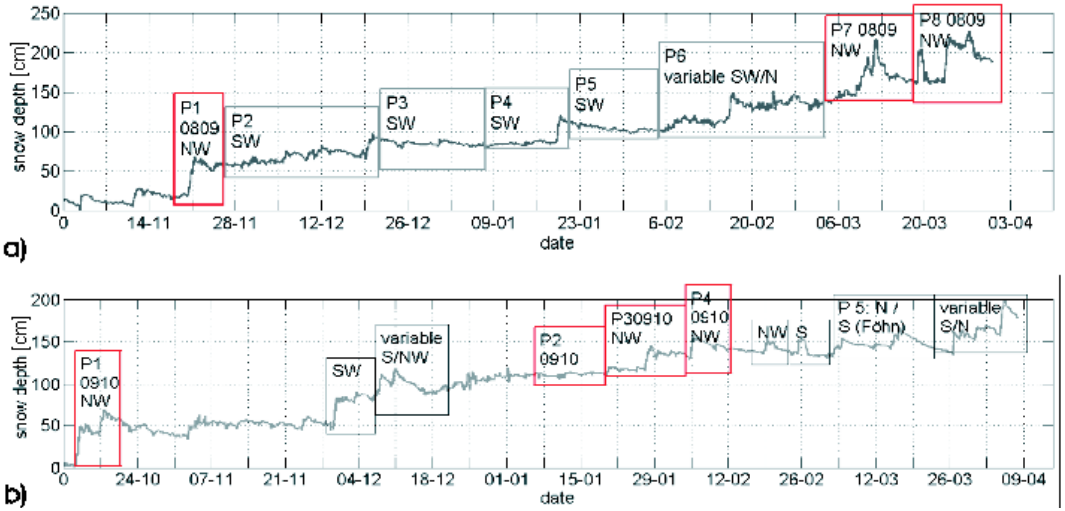

Fig. 2. Time series of snow-depth development during the accumulation seasons 2008/09 **(a)** and 2009/10 **(b)** at WAN7. Snow-drift events are marked with boxes. Measured snow-drift events are additionally marked with P, and those events referred to in the paper are indicated in red.

TCD
4, 865–900, 2010

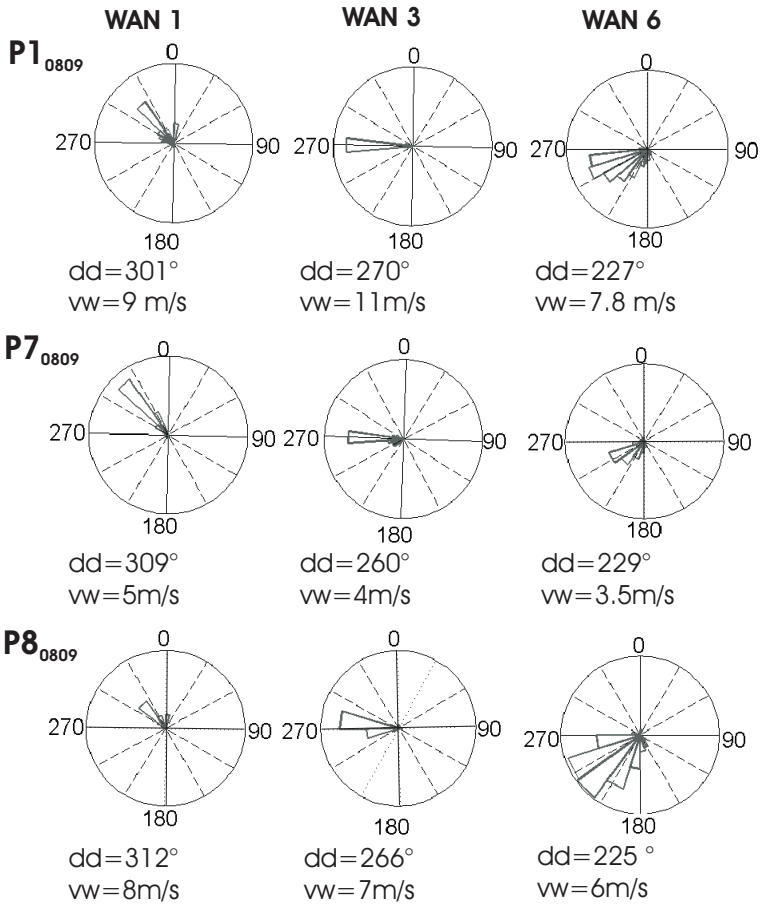

Fig. 3. Wind roses for the permanent weather stations WAN1, WAN3 and WAN6 for the three NW storms $P1_{0809}$, $P7_{0809}$ and $P8_{0809}$. d_d stands for the mean wind direction and and v_w for the mean wind velocity of the entire periods.

TCD
4, 865–900, 2010

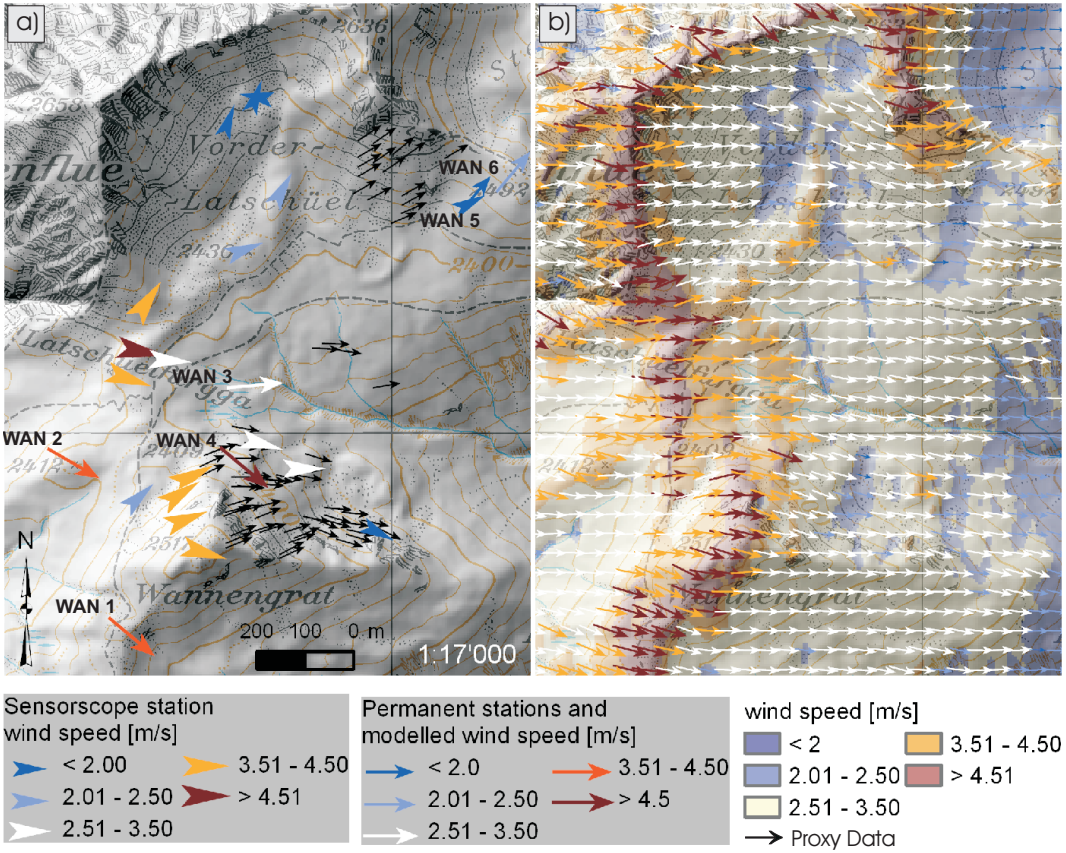

Fig. 4. Wind field measured by SensorScope and permanent stations **(a)** averaged for 24 h (28 January 2010, $P3_{0910}$). Proxy data from snow-surface structures measured after the snow fall event $P1_{0910}$ are shown by black wind vectors. Modelled wind field initialized with 2 m/s at 2400 m a.s.l. **(b)**. Note that the grid spacing of the model results was originally 5 m, but only one vector every 30 m is illustrated.

TCD
4, 865–900, 2010

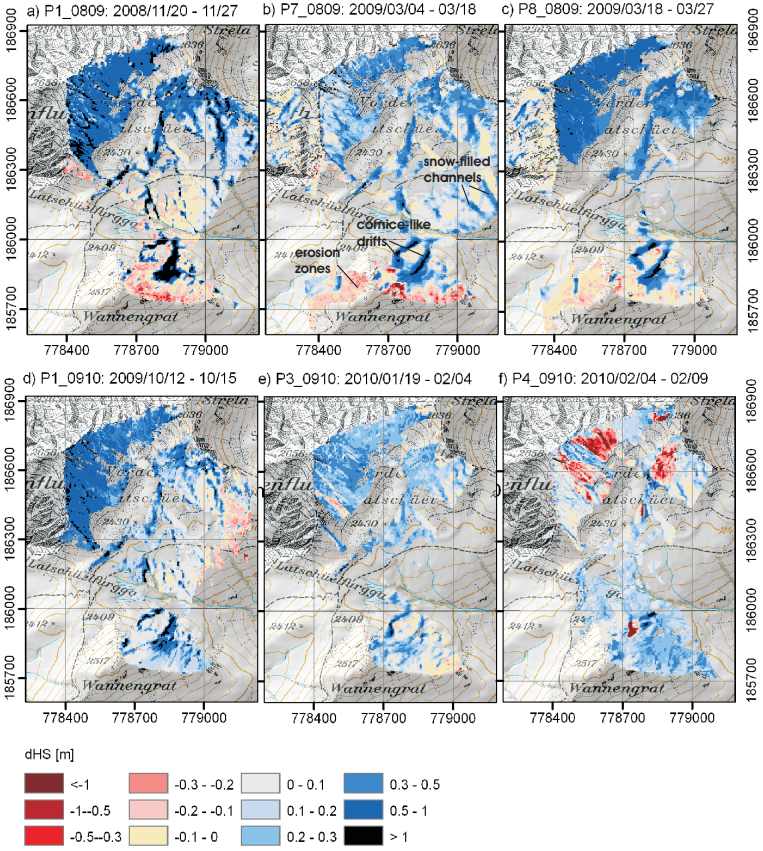

Fig. 5. Measured changes in snow depth (dHS) for the three major snow drift events in 2008/2009 and 2009/2010 during NW storms with precipitation. The horizontal grid resolution of snow-depth measurements were aggregated (mean) to a 5 m grid.

TCD
4, 865–900, 2010

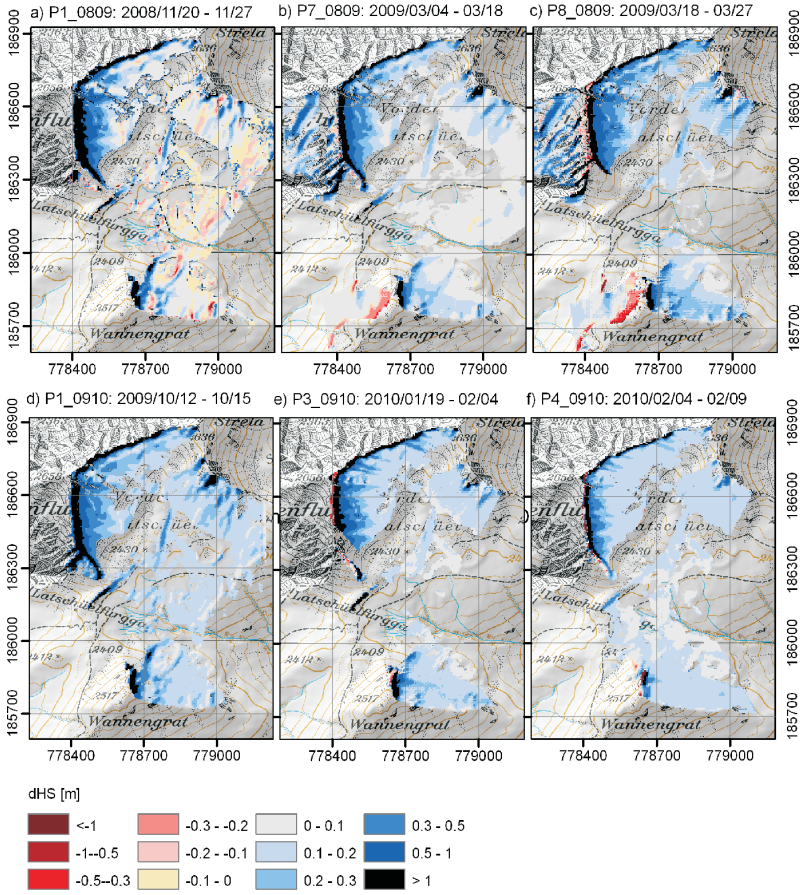

Fig. 6. Modelled changes in snow depth (dHS) for the three major snow-drift events in 2008/2009 and 2009/2010 for north-west wind. The domain of measurements was applied as a mask. The horizontal grid resolution is 5 m.

TCD
4, 865–900, 2010

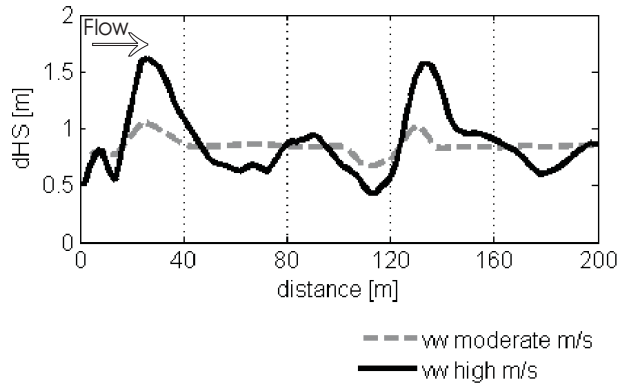

Fig. 7. Transects of modelled dHS crossing the two cross-slope ridges in flow direction, caused by high (initialized v_w=7 m/s) and moderate (initialized v_w=4 m/s) wind speeds. The transect is indicated in Fig. 1, lowest transect.

TCD
4, 865–900, 2010

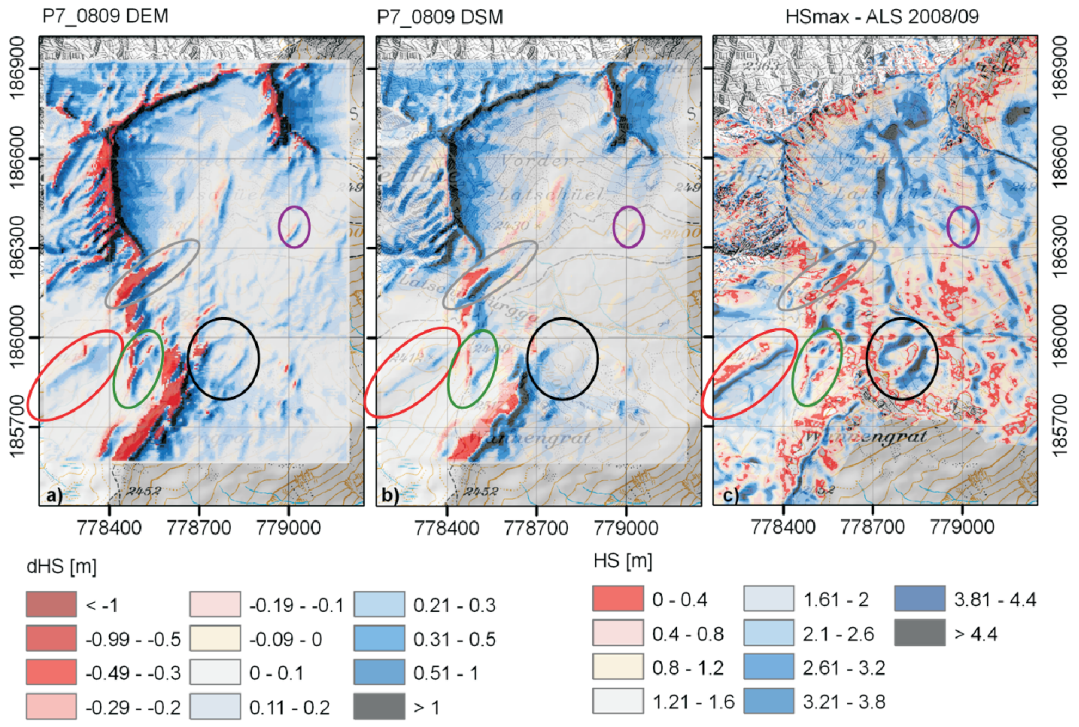

Fig. 8. Modelled changes in snow depth (dHS) for $P7_{0809}$ using DEM_S **(a)** and DEM_W **(b)** for the whole model domain. Horizontal grid resolution is 5 m. Measured snow depths (HS_{max}) 2008/09 (9 April 2009) with airborne laser scans with a horizontal resolution of 1 m **(c)**. Circles indicate consistent deposition patterns.

TCD
4, 865–900, 2010

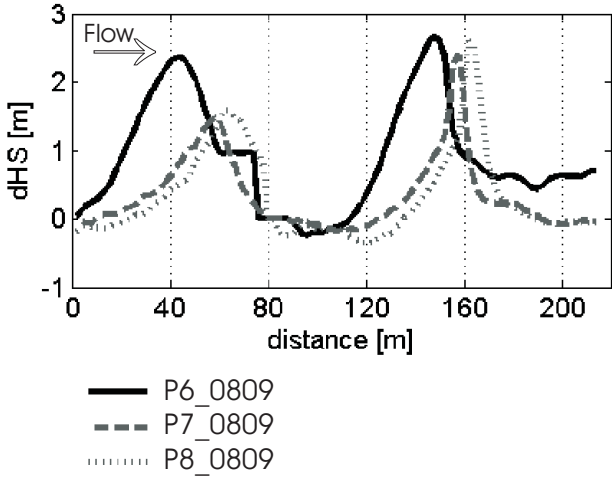

Fig. 9. Transect of measured dHS for periods 6, 7 and 8. Transect is shown in Fig. 1, lowest transect. Transect crosses the cornice-like drifts in flow direction, from northwest to southwest.

TCD
4, 865–900, 2010

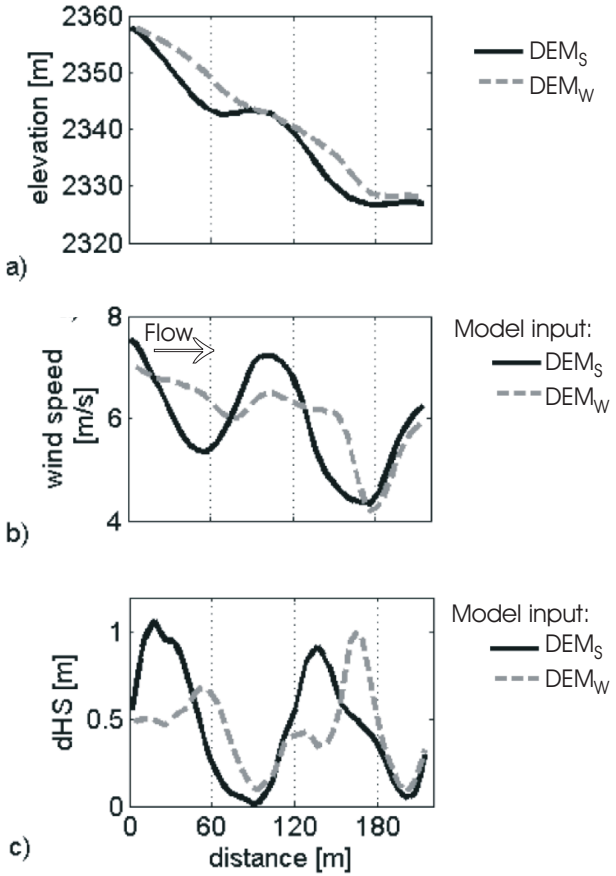

Fig. 10. Transects of summer (DEM$_S$) and winter topography (DSM$_W$) **(a)**, modelled three-dimensional wind speed **(b)** and modelled dHS **(c)** for P1$_{0708}$ (DEM$_S$) and P8$_{0708}$ (DEM$_W$). Transect is indicated in Fig. 1, lowest transect. Transect crosses the cornice-like drifts in flow direction, from northwest to southwest.

TCD
4, 865–900, 2010

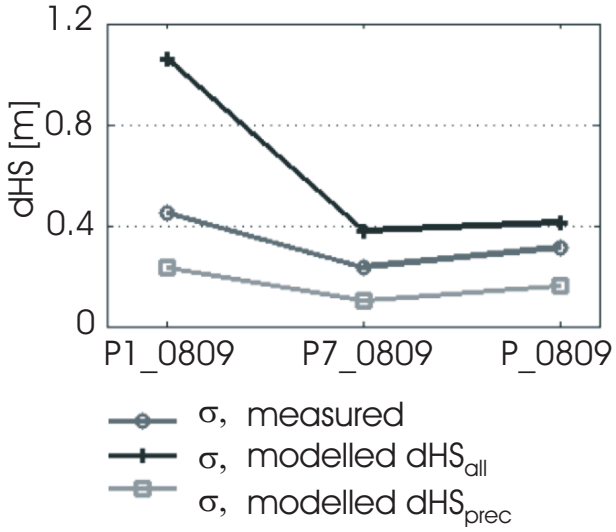

Fig. 11. Standard deviation of measured and modelled changes in snow depth (scanned area). Simulations were run with either all wind-induced snow-transport processes (dHS$_{all}$) or with preferential deposition of precipitation (dHS$_{prec}$) only.

TCD
4, 865–900, 2010

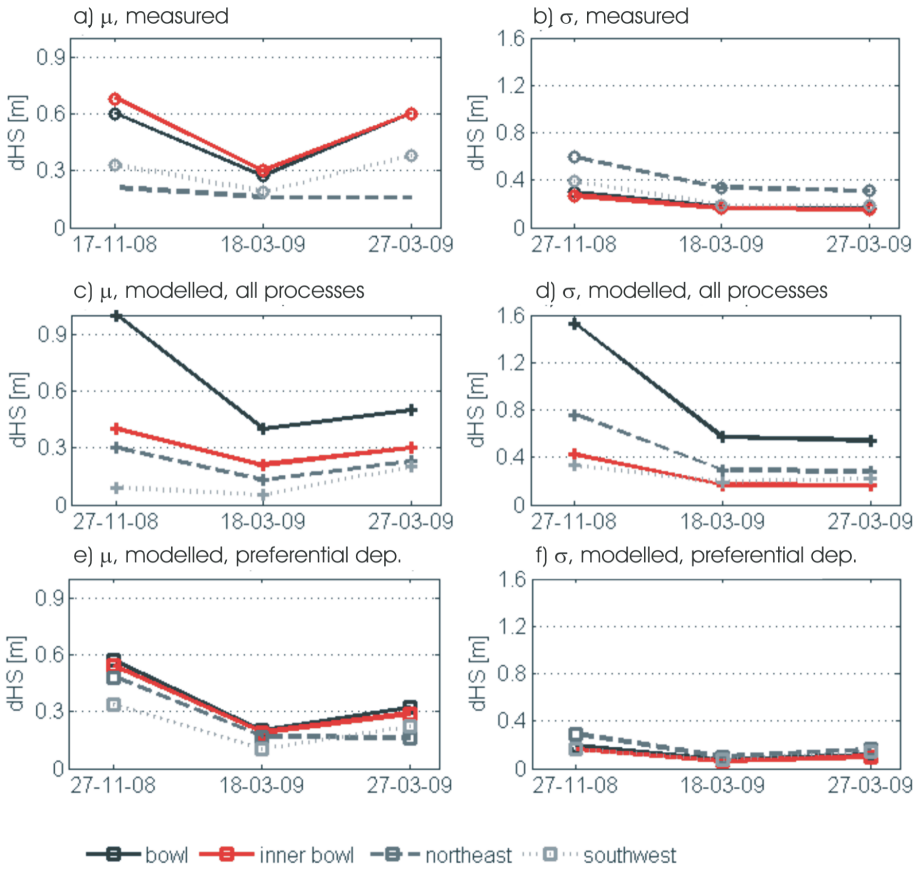

Fig. 12. Mean values **(a,c,e)** and standard deviation **(b,d,f)** for measured and modelled dHS for four sub-areas. Modelled dHS were derived from simulations where all wind-induced snow-transport processes were calculated (c,d), and where only the preferential deposition of precipitation was simulated (e,f).

TCD
4, 865–900, 2010

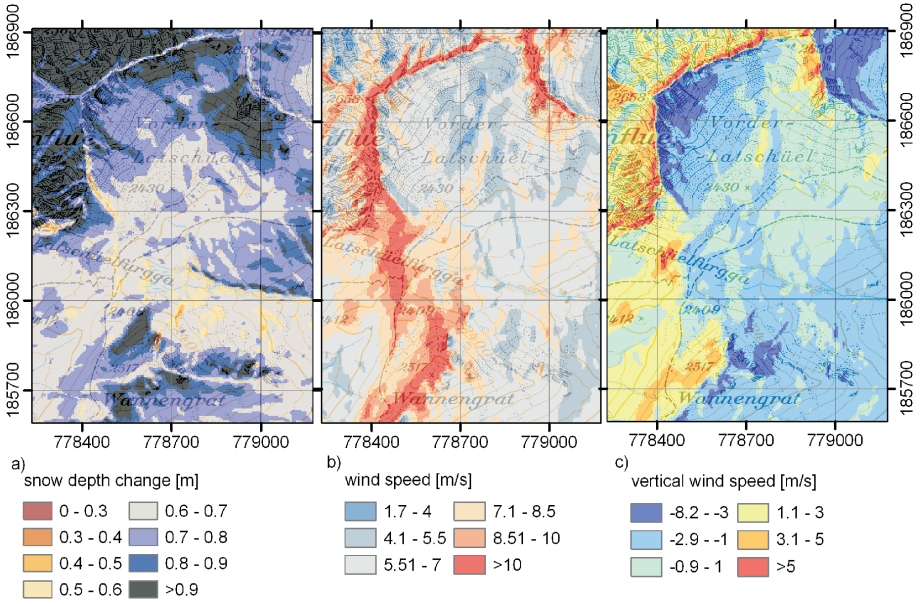

Fig. 13. (a) Changes in Snow depth (dHS_{prec}) due to preferential deposition of snow for $P1_{0809}$, **(b)** wind speed and **(c)** vertical component of wind speed.

TCD
4, 865–900, 2010